Monthly Notices of the ROYAL ASTRONOMICAL SOCIETY

MNRAS **504,** 5919–5926 (2021) doi:10.1093/mnras/stab1241
Advance Access publication 2021 May 4

The influence of the spiral arm parameters on radial migration in late-type-like galaxies

Gerardo Martínez-Bautista,[1★] Héctor Velázquez,[1★] Angeles Pérez-Villegas [2★] and Edmundo Moreno[1]

[1] *Instituto de Astronomía, Universidad Nacional Autónoma de México, A.P. 70-264, 04510 Ciudad de México, México*
[2] *Instituto de Astronomía, Universidad Nacional Autónoma de México, A.P. 106, C.P. 22800 Ensenada, B.C., México*

Accepted 2021 April 27. Received 2021 April 26; in original form 2021 March 22

ABSTRACT

We performed test-particle simulations of a spiral late-type-like galaxy to study the radial migration in a steady potential. Our model includes a bulge, a disc, a dark matter halo, and spiral arms represented by a cosine potential. We varied the structural and dynamical parameters of the spiral arms to study the influence of each configuration on the stellar orbits, such as the pitch angle, the radial scale length, and the pattern speed. We analysed the changes in the z component of the angular momentum (L_z), radius (R), and eccentricity of individual stars at different times. We found that the stellar orbits are affected by radial migration in all cases. Also, we found that the most relevant parameter to the radial migration phenomenon, in co-rotation, is the radial scale length of the spiral arms.

Key words: galaxies: disc – galaxies: kinematics and dynamics – galaxies: spiral – galaxies: structure.

1 INTRODUCTION

Spiral arms are one of the most striking and intriguing features in spiral galaxies. In recent years, there has been an intensive ongoing research in this field to have a better understanding why different spiral patterns are observed, spanning from flocculent, great design, and bisymmetric structures (e.g. Hart et al. 2018, and references therein). In a dynamical context, spiral arms play a relevant role in the stellar orbital dynamics by modifying the angular momentum, leading to some stars moving several kpc beyond the place where they were born, and/or by heating up the stellar disc (Edvardsson et al. 1993; Wielen, Fuchs & Dettbarn 1996). In a seminal work, Sellwood & Binney (2002) proposed a dynamical mechanism for explaining this physical process, the so-called radial mixing, which results from the interaction, in co-rotation (CR), of a perturbing potential, like a spiral arm, on the stellar orbits that move in a smooth galactic axisymmetric potential.

The basic mechanism consists in that a change in the specific orbital angular momentum in the z component, L_z, can be only driven by non-axisymmetric forces, like spiral arms, bars, or molecular clouds. The radial mixing is divided into two branches: 'churning', which means a change in L_z but not in the eccentricity of the stellar orbit, which is commonly referred to as radial migration, and 'blurring' implying changes in both L_z and eccentricity, and it is known as dynamical stellar heating or simply heating (Schönrich & Binney 2009).

However, it should be pointed out that in the literature there is not a general consensus on the definition of radial migration. Some authors consider that radial migration is a change in L_z but without a change in the orbital eccentricity (Vera-Ciro et al. 2014; Loebman et al. 2016; Martinez-Medina et al. 2016); none the less, blurring is considered by some as migration (Minchev & Famaey 2010). In this work, we will adopt the radial migration as a churning mechanism (Sellwood & Binney 2002; Schönrich & Binney 2009).

The study of radial mixing with restricted simulations using a steady galactic model with the spiral arms represented by a cosine potential and/or also by including a quadrupole bar has been extensively used in the literature (Quillen et al. 2009; Monari, Famaey & Siebert 2016a; Monari et al. 2016b; Hunt & Bovy 2018; Hunt et al. 2018a,b, 2019). In particular, Minchev & Famaey (2010) found that the overlapping of resonances is a more efficient mechanism than transient spiral arms alone to mix material due to stellar radial migration along the regions where this overlapping occurs in the disc. Similar results have been found by Martinez-Medina et al. (2016) employing spiral arms and bar models based on a mass distribution for these components (Pichardo et al. 2003; Pichardo, Martos & Moreno 2004). However, more detailed N-body + smoothed particle hydrodynamics (SPH) simulations show that these transient spiral arms could develop different pattern speeds, moving the CR radius in a more wider region of the disc giving rise to radial migration in this more ample region (Grand, Kawata & Cropper 2012). Also, in models with a bar where the slowdown of the bar pattern speed moves CR radius outwards they produce radial migration towards external regions of the disc (Halle et al. 2018).

Both radial migration and heating are not processes that can be measured directly; for this, we must resort to indirect studies through the metallicity distribution function (MDF hereafter). Recent surveys such as APOGEE for the Milky Way (Eisenstein et al. 2011) and CALIFA for external galaxies (Mejía-Narváez et al. 2020) have been measuring the stellar metallicity (Eisenstein et al. 2011) due to the information that can be extracted from the shape, skewness, and the extent of the MDF of a galaxy, giving us an insight about how radial migration has occurred (Hayden et al. 2015; Aumer, Binney & Schönrich 2016; Loebman et al. 2016; Martinez-Medina et al. 2017).

★ E-mail: gmartinez@astro.unam.mx (GM-B); hmv@astro.unam.mx (HV); mperez@astro.unam.mx (AP-V)

Furthermore, local chemo-kinematics studies near the disc plane of the Milky Way show that the thin disc component has stars of all ages at large radii with a positive [Fe/H] skewness in the outskirts, suggesting that radial migration has a relevant role in the metallicity scatter of the thin disc (Grieves et al. 2018).

In an *N*-body simulation of a Milky Way-like galaxy, it is found that stars with very eccentric orbits in the central region can be tossed several kpc outwards near the bar outer Lindblad resonance (OLR) and they are circularized after a few Gyr, so it can be seen as an 'inverse process to heating' (Halle et al. 2018; Khoperskov et al. 2020). Also, particles with a low eccentricity and lagging a short-lived local density peak can migrate outwards of the disc (Comparetta & Quillen 2012). The spiral arms induce an increase of the vertical velocity dispersion of the stars. However, this vertical heating is small and it does not account for the thickening of the disc, and hence the formation of the thick disc; even more, stars with very large vertical velocity dispersion are less prone to radially migrate (Vera-Ciro et al. 2014; Vera-Ciro, D'Onghia & Navarro 2016; Mikkola, McMillan & Hobbs 2020). In addition, it is seen in *N*-body Tree/SPH simulations that, in the presence of a bar, the vertical velocity dispersion of inward migrating populations is smaller than that of the non-migrating populations; therefore, the inward migrating stars have a negative contribution to the vertical heating by 'cooling' the disc at smaller radii than at the CR position of the bar (Minchev et al. 2012b). On the other hand, Roškar et al. (2011) suggested that radial migration would be a natural mechanism to contribute to the formation of the thick disc in the sense that despite the radial velocity dispersion is not increased, the migrating stellar population conserves its vertical energy and, at larger radii, the disc surface falls and in consequence its restoring force decreases. This could cause an increase in the vertical oscillations, favouring the formation of the thick disc.

On the observational side, data have accumulated in recent years indicating that this mechanism of radial migration has been working in our Galaxy and external galaxies. Radial metallicity gradients are of particular interest because they clearly can show the process of radial migration. Some simulations have shown that the initial radial metallicity gradient flattens due to the radial mixing produced by the bar and spiral arms (Minchev et al. 2012a). In particular, if the spiral structure is transient, this defines a CR region where stars may move from one radius to another, reaching up to 5 kpc in less than 0.5 Gyr (Roškar et al. 2011).

In simulations of restricted test particles, of a Milky Way-like model, with transient spiral arms and different pattern speeds, it is found that stars in CR, in addition to experiencing radial migration, also experience radial heating due to the overlap of ultra-harmonic resonances (Daniel et al. 2019). About 40 per cent of the stars in the solar neighbourhood have experienced both radial migration and heating by this overlapping of resonances. Furthermore, in a previous work, Klačka, Nagy & Jurči (2012) indicated that the Sun has migrated at most 1.2 kpc due to the action of spiral arms; however, recent numerical simulations suggest that these non-axisymmetric perturbations have caused a displacement of the Sun of around 3 kpc from its current position due to radial migration (Tsujimoto & Baba 2020).

Using observational data from the AMBRE project (de Laverny et al. 2013) and a semi-analytical model for the Milky Way (Kubryk, Prantzos & Athanassoula 2013), Prantzos et al. (2017) were able to explain the behaviour of the Li/H double branch versus metallicity observed in the local thin and thick disc components as a result of radial migration. Also, by combining the radial information and velocities from the second *Gaia* data release (DR2; Gaia Collaboration 2018) and assuming that it is possible to infer the formation radius of a sample of the branch of the red giants, it is found that some stars have experienced churning or blurring. From this sample, about 10 per cent have experienced radial migration while about 5–7 per cent of them have never been affected by this process (Feltzing, Bowers & Agertz 2020).

Through a galactic surface brightness study using a sample of the CALIFA survey, made by Ruiz-Lara et al. (2017), it is found that radial migration mixes the stellar content, flattening the radial stellar properties such as light, age, and metallicity distributions. However, it strongly depends on the disc characteristics of each galaxy. The authors also suggest that processes like star formation or accretion might be as important as radial migration in the mixing of the stellar properties. In an oxygen abundance study in a sample of spiral galaxies from MUSE, Sánchez-Menguiano et al. (2018) found that some of them have lower (higher) oxygen abundances in the inner (outer) regions than the expected distribution. Even more, they show a large dispersion in the slope distribution of these abundance gradients. Also, Zhuang et al. (2019) investigated the influence of radial migration due to a bar and the spiral arms in the stellar populations, using the radial stellar metallicity information, in a sample of 244 galaxies from CALIFA. They found that radial migration seems to play a secondary role since there is not a strong correlation among its effects and the stellar population gradients.

In order to study the possible influence of radial migration in late-type galaxies, we performed a series of simulations varying the structural and dynamical parameters of the spiral arms. This work is organized as follows. In Section 2, we describe our adopted late-type galaxy and spiral arms models. Section 3 presents the results of our simulations. Finally, a discussion and conclusions are drawn in Section 4.

2 TEST-PARTICLE SIMULATIONS

With the aim to study the influence of the spiral arms parameters on a late-type galaxy, we carry out simulations with test particles. For the sake of clarity, we briefly describe below the models used for this work.

2.1 The model for late-type galaxies

The galactic model for the late-type galaxy is represented by a 3D steady state composed potential. It consists of a Plummer profile with a mass of $M_{\rm B} = 10^{10}$ M$_\odot$ and a scale length $r_{\rm B} = 1$ kpc for the bulge (Plummer 1911), a Miyamoto–Nagai distribution for the disc with a mass $M_{\rm D} = 5.1 \times 10^{10}$ M$_\odot$ and with the scale lengths $a = 5.31$ kpc and $b = 0.25$ kpc, respectively (Miyamoto & Nagai 1975). For the halo, we adopted a Hernquist profile with a mass of $M_{\rm H} = 4.8 \times 10^{11}$ M$_\odot$ and a scale length of $r_{\rm H} = 33$ kpc (Hernquist 1990). The contribution of each component to the rotation curve of the model is shown in the upper panel of Fig. 1.

Following Contopoulos & Grosbol (1986), we represent the spiral arms by the cosine potential:

$$\Phi_{\rm spiral}(R, \phi, z) = f(R)\cos[2\phi + g(R)]{\rm sech}^2\left[\frac{z}{z_0}\right], \quad (1)$$

where (R, ϕ, z) are the cylindrical coordinates in a non-inertial reference frame rotating with the spiral arms, $f(R) = -AR\exp(-R/R_{\rm sp})$ is the amplitude function of the perturbation being A and $R_{\rm sp}$ the amplitude and radial scale length of the spiral arm. The vertical contribution to the potential was taken from Patsis & Grosbol (1996).

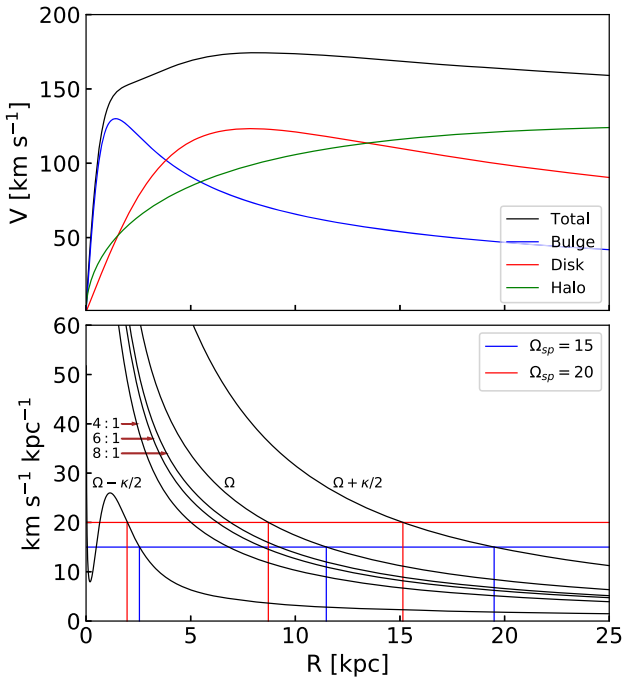

Figure 1. Top panel shows the rotation curve of our late-type galaxy model for the axisymmetric background potential. Bottom panel shows the resonance positions of the model for the two pattern speeds used in this work.

Table 1. Values for the parameters of the spiral arms model adopted in this work to study their role in the radial migration in the disc.

	Spiral arms parameters			
Parameter	A	B	C	D
R_{sp} (kpc)	5.31	6.64	5.31	5.31
i_p (°)	20	20	40	20
Ω_{sp} (km s^{-1} kpc^{-1})	15	15	15	20
A (km^2 s^{-2} kpc^{-1})	650	650	650	650

The geometry of the spiral pattern (*locus*) is given by

$$g(R) = -\frac{2}{N \tan i_p} \ln[1 + (R/R_s)^N], \tag{2}$$

where i_p is the pitch angle, R_s is the start position for the spiral arms, and N is a constant that shapes the starting point of the spiral arms (Roberts, Huntley & van Albada 1979). In this work, N is set to 100 (see Pichardo et al. 2003 for more details).

In this work, we study four models where we vary some of the relevant parameters of the spiral arms potential such as the radial scale length, R_{sp}, the patter speed, Ω_{sp}, and the pitch angle, i_p. In all these cases the amplitude was kept fixed and equal to $A = 650$ km^2 s^{-2} kpc^{-1}. In Fig. 1, we have summarized the different parameter values for the spiral arms models where, we have adopted Model A as our fiducial model. All models share the same axisymmetric background galactic potential. The values for the radial scale length of the spiral arms, R_{sp}, in Fig. 1 are consistent with the results of the work of Mata-Chávez et al. (2019) who found that this scale is larger by 5– 40 per cent than the radial scale length of the disc of a Milky Way-like galaxy. Also, for the pitch angle we included a maximum value of $i_p = 40°$ (Ma et al. 2000; Yu & Ho 2020) since larger values may lead to a model dominated by chaotic orbits, if the chaotic behaviour becomes pervasive, the orbits supporting the spiral arms will be destroyed (Pérez-Villegas et al. 2012; Pérez-Villegas, Pichardo & Moreno 2013, 2015). Meanwhile, the pattern speed values are consistent with the results by Fathi et al. (2009). Bottom panel of Fig. 1 shows the positions of the different resonances for our galaxy model. The blue line corresponds to spiral arms with a pattern speed of $\Omega_{sp} = 15$ km s^{-1} kpc^{-1} while the red line to a pattern speed of $\Omega_{sp} = 20$ km s^{-1} kpc^{-1}, and when $\Omega_{sp} = \Omega - \frac{\kappa}{2}$, $\Omega_{sp} = \Omega + \frac{\kappa}{2}$, and $\Omega_{sp} = \Omega$, the positions of the Inner Lindblad Resonance (ILR), the OLR, and the CR resonance are fixed, respectively. Table 1 gives the spiral arms parameters of our models.

The equations of motion are solved in the non-inertial reference frame system, rotating with a constant angular velocity given by the spiral arms pattern speed Ω_{sp}. The orbits of the test particles in this galaxy potential model are followed by 5 Gyr using a Runge–Kutta integrator (Press et al. 1992) with a Jacobi energy conservation better than 10^{-14}. In all cases, the spiral arms are grown adiabatically during the first Gyr, to avoid a non-negligible transient response of the orbits resulting from an abrupt introduction of this non-axisymmetric perturbation that may lead to a spurious radial migration.

2.2 Initial conditions for test particles

To specifying the positions and velocities of the disc test particles, we resort to the work of Hernquist (1993), a technique resting in Jeans equations and for sake of completeness we describe it briefly below.

Test particle positions are drawn from the Miyamoto–Nagai disc distribution and to determine their velocities we employ the second moment of the Collisionless Boltzmann Equation for an axisymmetric distribution:

$$v_c^2 - < v_\phi >^2 = \sigma_\phi^2 - \sigma_R^2 - \frac{R}{\Sigma} \frac{\partial(\Sigma \sigma_R^2)}{\partial R}, \tag{3}$$

where it has been assumed that the velocity ellipsoid is aligned with the coordinate axes. This expression can be simplified even further by assuming:

$$\sigma_R^2(R) \propto \Sigma(R), \tag{4}$$

and that the azimuthal dispersion is given by the epicyclic approximation as

$$\sigma_\phi^2(R) = \sigma_R^2 \frac{\kappa^2}{4\Omega^2}, \tag{5}$$

where κ and Ω are the epicycle and angular frequency, respectively.

With these assumptions, equation (3) reduces to

$$v_c^2 - < v_\phi >^2 = \sigma_R^2 \left[\frac{\kappa^2}{4\Omega^2} - 1 - 2 \frac{\partial(\ln \Sigma)}{\partial \ln R} \right]. \tag{6}$$

The radial dispersion velocity can be specified to a given radius, $R_\bullet$, using the Toomre Q parameter as a constraint

$$\sigma_R(R_\bullet) = Q_\bullet \frac{3.36 G \Sigma}{\kappa^2}, \tag{7}$$

we take $Q_\bullet = 1.2$ at $R_\bullet = 2a$ to ensure local stability. The vertical dispersion is given by

$$\sigma_z^2 = \pi G \Sigma(R) b. \tag{8}$$

Finally, the Cartesian velocities can be obtained from Gaussian distributions with dispersions σ_z, σ_R, and σ_ϕ and combining

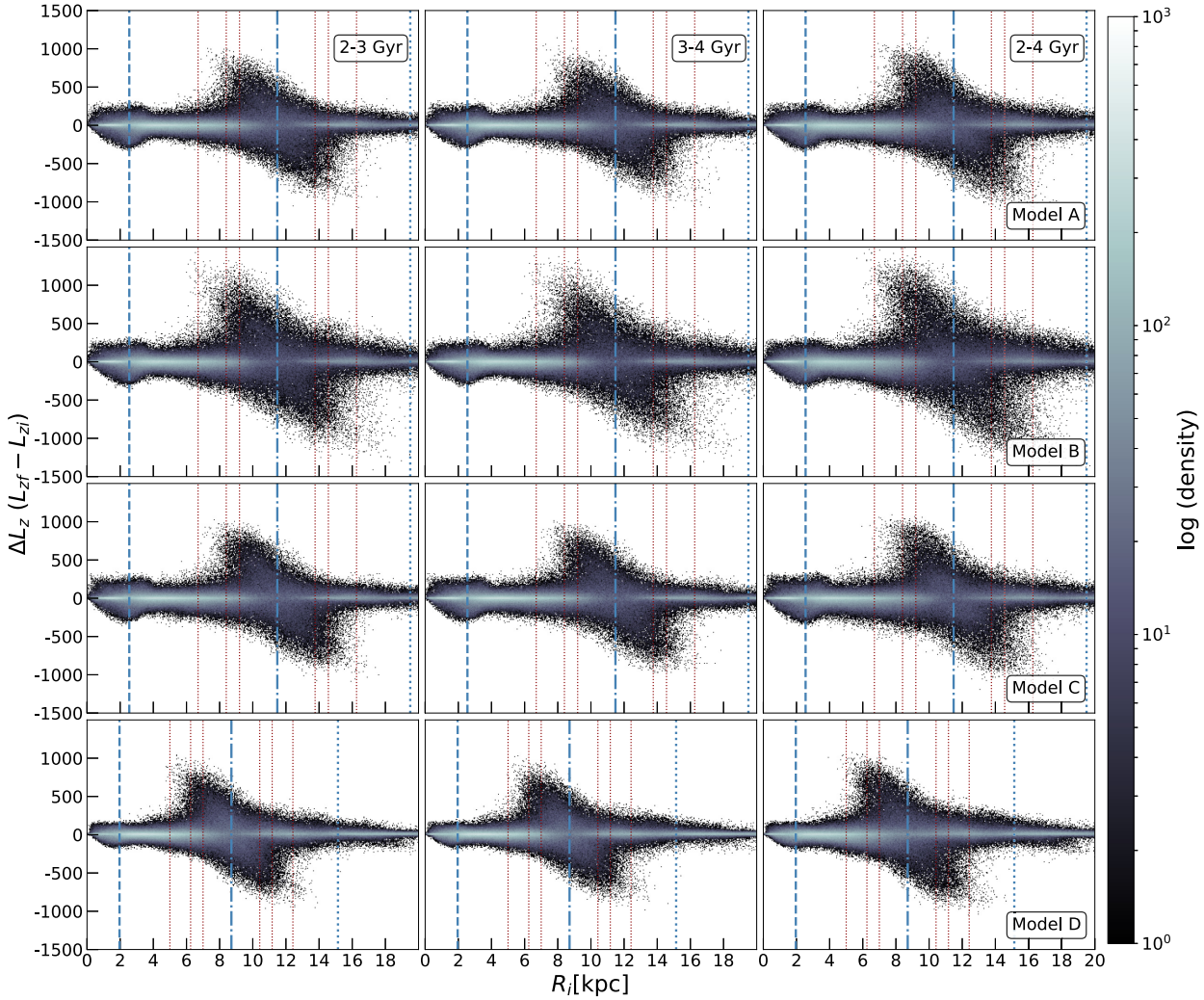

Figure 2. Changes in L_z, given in kpc km s^{-1}, for three different intervals of time (columns). Rows correspond to Models A, B, C, and D, respectively. The blue dashed, dash–dotted, and dotted lines indicate the ILR, CR, and OLR positions of the galaxy, while the red dotted lines indicate the ultra-harmonic resonances (4:1, 6:1, 8:1, 1:8, 1:6, and 1:4, from left to right). The colour bar shows the particle density in a logarithm scale.

these last two with equation (6) to obtain the azimuthal streaming velocity.

3 RADIAL MIGRATION

In order to analyse the radial migration, we estimate the change in angular momentum in the z-component ($\Delta L_z = L_{z,f} - L_{z,i}$), radius ($\Delta R = R_f - R_i$), and eccentricity ($\Delta \mathrm{ecc} = \mathrm{ecc}_f - \mathrm{ecc}_i$) in an interval of time from t_i to t_f. For the eccentricity, we take the following expression (Arifyanto & Fuchs 2006; Minchev et al. 2012a)

$$\mathrm{ecc} = \sqrt{\frac{u^2 + \frac{\kappa^2}{\Omega^2} v^2}{r^2 \kappa^2}}, \tag{9}$$

where u is the radial velocity respect to the galactic centre, $v = V_c - V_\phi$ with V_c and V_ϕ the circular and tangential velocities, respectively, κ is the radial epicyclic frequency, Ω is the angular frequency, and r is de galactocentric distance.

Due to the cosine potential shows a spurious bar-like component in the central part which might cause non-physical variations of the eccentricity in the central region within 3 kpc, we avoid that region for our analysis.

3.1 Changes in L_z

Fig. 2 shows the ΔL_z as function of the initial galactocentric distance, R_i, for our models. From top to bottom, each row corresponds to the evolution of the different models as described in Section 2.1, and from left to right, each column shows ΔL_z between different time intervals 2–3 Gyr, 3–4 Gyr, and 2–4 Gyr.

For our fiducial model A (first line in Fig. 2), the particles showing larger changes in ΔL_z are seen around the CR region, where they are spread in a diagonal centred at this resonance, independently of the chosen time interval, with a maximum of $|\Delta L_z| \sim 1000$ kpc km s^{-1}. When the difference in time is 1 Gyr (two first panels), the ΔL_z seems to have a similar behaviour, but for the difference in time of 2 Gyr (third panel), the accumulative effect could be the responsible of the larger changes seen in ΔL_z and the spread in R_i.

Looking at Model B, for which the radial scale, R_{sp}, of the spiral arms has been increased by around 25 per cent with respect to the fiducial model A (second line in Fig. 2), it shows an increase in ΔL_z, clearly exceeding the maximum value found in Model A, no matter the time. Around CR, not only larger changes in ΔL_z than in model A occur, but also a larger spread in R is seen. In the surrounding of CR, a zone of dispersed particles is formed.

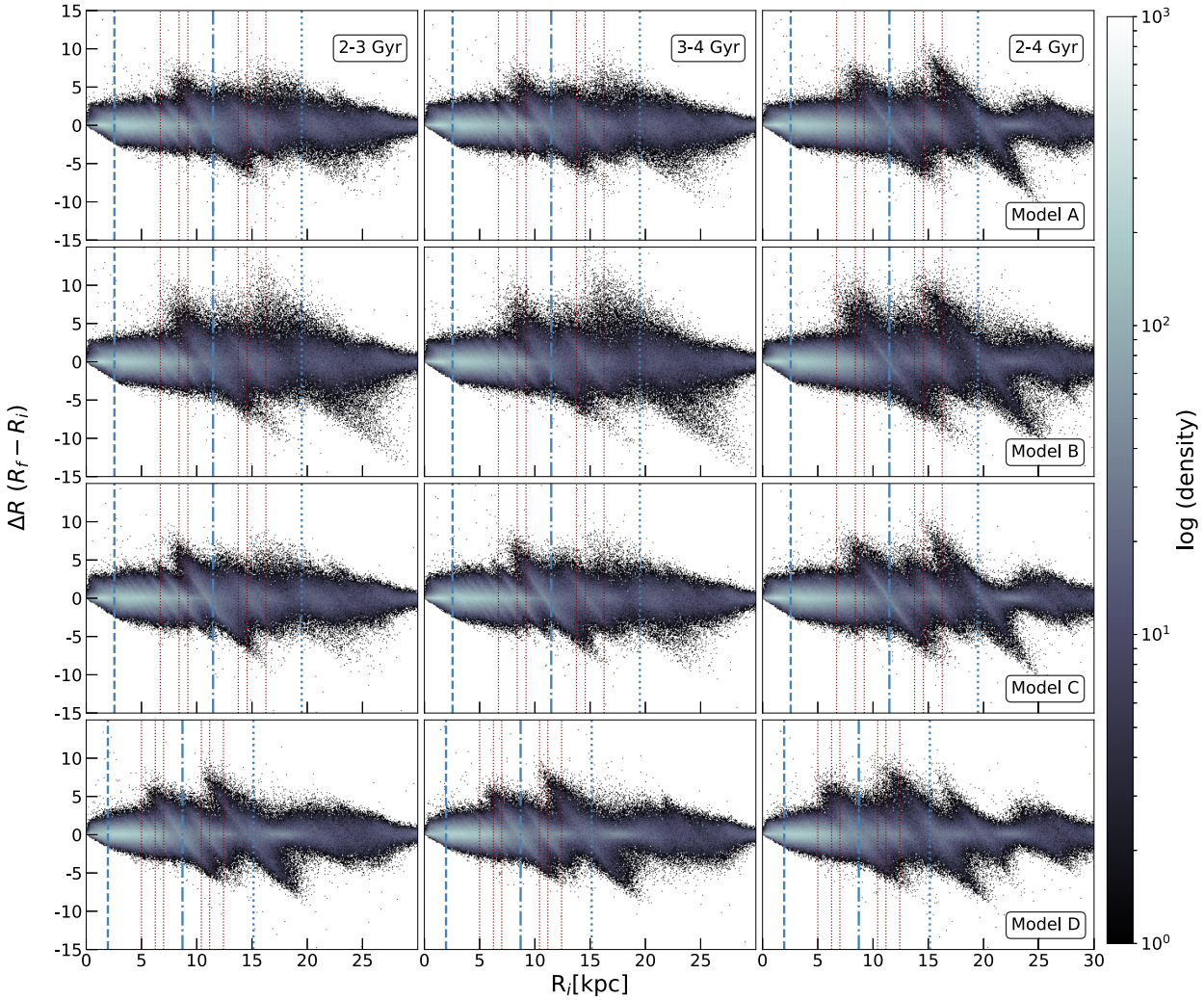

Figure 3. Changes in R, given in kpc, for three different intervals of time (columns). Rows correspond to Models A, B, C and D, respectively. The blue dashed, dash–dotted, and dotted lines indicate the ILR , CR, and OLR positions of the galaxy, while the red ones designate the ultra-harmonic resonances (4:1, 6:1, 8:1, 1:8, 1:6, and 1:4, from left to right).

Regarding Model C, which has a pitch angle larger by a factor of two with respect to the fiducial model A (third line in Fig. 2), ΔL_z seems to have a similar evolution for all the considered time intervals and is only slightly larger than the changes shown in Model A. Finally, for Model D, similar to the fiducial Model A but with a larger patter speed, Ω_{sp}, for the spiral arms (fourth line in Fig. 2), we can see that $|\Delta L_z|$ is similar to the one observed in the CR of Model A. Notice that the location of the CR radius is closer to the centre and they cannot be compared directly, however, the overall behaviour is similar.

3.2 Changes in R

Fig. 3 is similar to Fig. 2, but it shows the change in radii, ΔR, of the stellar orbits. In the first row (our fiducial Model A), ΔR is larger than 5 kpc for time intervals of 1 Gyr around CR and the OLR and less than 5 kpc in other regions. The cumulative effect in two Gyr is clearly seen in the third panel, where ΔR can reach up to 10 kpc in the OLR region. It seems that OLR has stronger effect compared to CR, however, the number of particles spread in OLR is fewer than in CR. Those large displacements were also observed in *N*-body simulations, where particles with very high radial migration were called 'extreme migrators' by Halle et al. (2018). In particular, in those simulations, this behaviour was attributed to the bar OLR, while for our simulations, these are due to the spiral arms. For all times, ridges are connected with the position of the resonances, where the larger displacement is observed.

For Model B (second row), ΔR is bigger than in our fiducial Model A. In these panels, particles near CR and OLR can travel more than 10 kpc (inward or outward), these displacements are significantly larger than those observed in Model A. On the other hand, both Models C and D show a similar global behaviour than Model A, with small differences. For instance, the ridges around the resonances in Model C are more well defined than in Model A while, in Model D, the change ΔR in the OLR is larger than in the region around CR.

Despite all parameters of the spiral arms play a role in the process of radial migration, clearly, the most relevant is the radial scale length R_{sp} of the spiral arms pattern (Model B), leading to larger changes in ΔL_z and ΔR as is shown in the results of Figs 2 and 3, respectively.

3.3 Changes in eccentricity

To disentangle between radial migration and radial heating, we determine the change in eccentricity as defined in equation (9). Fig. 4

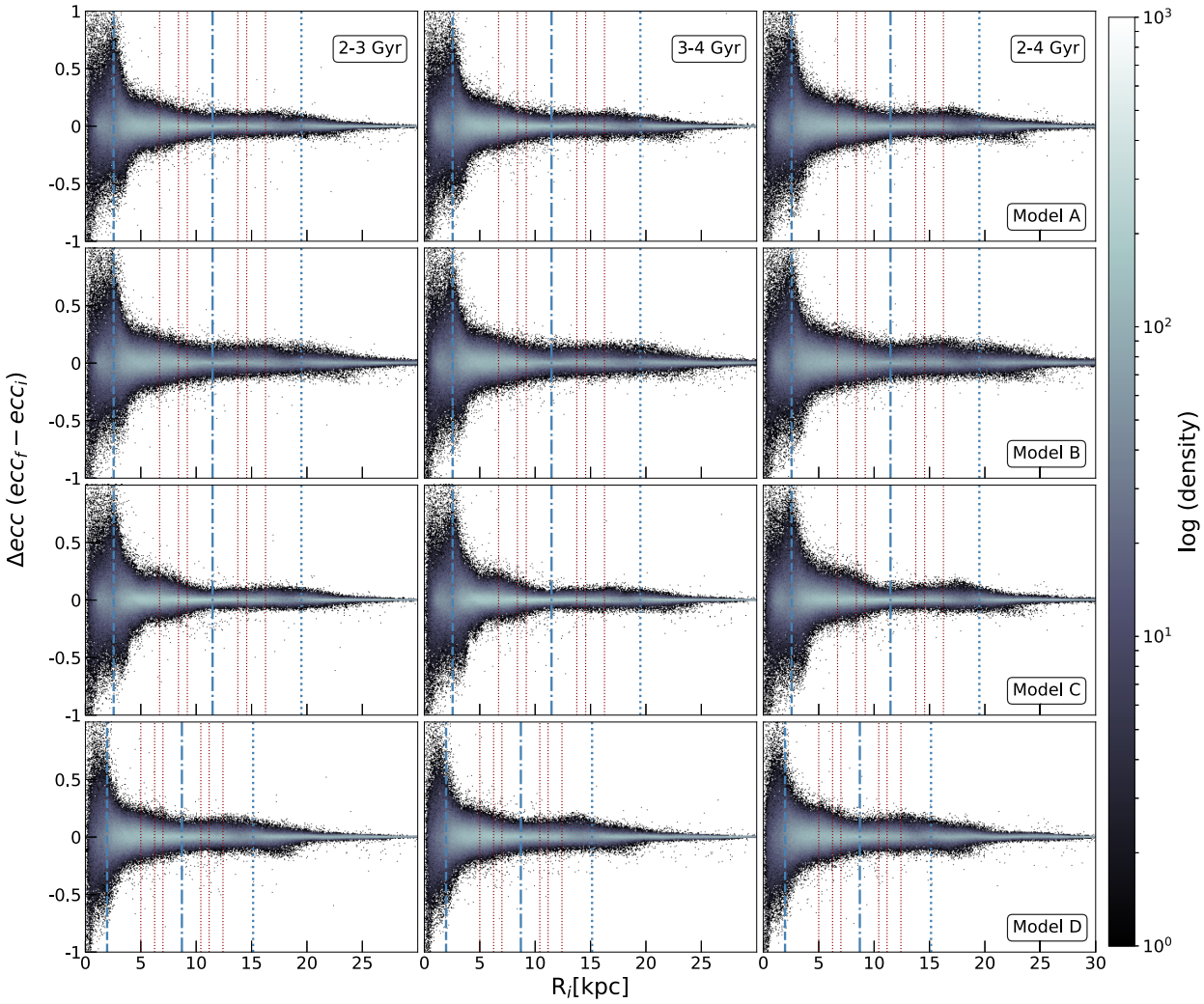

Figure 4. Changes in eccentricity for three different intervals of time given by the columns as in Fig. 2. Rows indicate Models A, B, C, and D. The blue dashed, dash–dotted, and dotted lines are the ILR, CR, and OLR positions of the galaxy, while the red ones designate the ultra-harmonic resonances (4:1, 6:1, 8:1, 1:8, 1:6, and 1:4, from left to right).

shows Δecc as a function of the initial radii R_i at the same three time intervals shown in Figs 2 and 3. It can be seen that in the central region Δecc increases by large values but it is due, in part, to the cosine spiral arms model since it has a non-physical bar-like behaviour and, for our purposes, this region is ignored. However, for all models around CR, we can observe large changes in L_z (Fig. 2) but small changes in ecc (Fig. 4) in CR and other resonances like the OLR, indicating that the stellar orbits can move inwards or outwards preserving nearly circular orbits which is precisely the mechanism of radial migration.

3.4 Quantifying the changes

In order to quantify the effect of modifying the value of the parameters of the spiral arms in the radial migration, we analyse the initial and the final position of each particle in our models. Fig. 5 shows the particle distribution from $t = 0$ to $t = 4$ Gyr. Each coloured 3 kpc-size bin represents the initial position of the particles, and the colour curves are the final particle distribution. Each curve is normalized to the number of particles in its corresponding bin at $t = 0$ Gyr. The solid, dashed, and dotted lines correspond to Model A, Model B, and Model C, respectively. For clarity, Model D is shown separately since the pattern speed of the spiral arms is larger in this case and hence the position of its resonances are closer to the central region (Fig. 5, bottom panel). It can be noticed from this figure that after 4 Gyr the shapes of the curves of the first bins closer to the inner region of the galaxy but not to CR are similar and roughly symmetrical suggesting that radial migration is small. However, the situation is completely different for the bins closer to the CR resonance, all the shapes of the curves show a positive (negative) skewness if the bin is before (after) the CR radius, indicating that radial migration is operating and moving particles to larger (smaller) distances from their original positions. This is particularly more clearly seen in Model B (dashed-line, upper panel of Fig. 5). Also, some positive skewness can be appreciated in Model D for the curve just before the OLR with particles moving up to 10 kpc. These results are in agreement with the results found in previous subsections. This skewness could be used to indirectly determine the position of the principal resonances and, if the rotation curve of the galaxy is known, the pattern speed could be estimated.

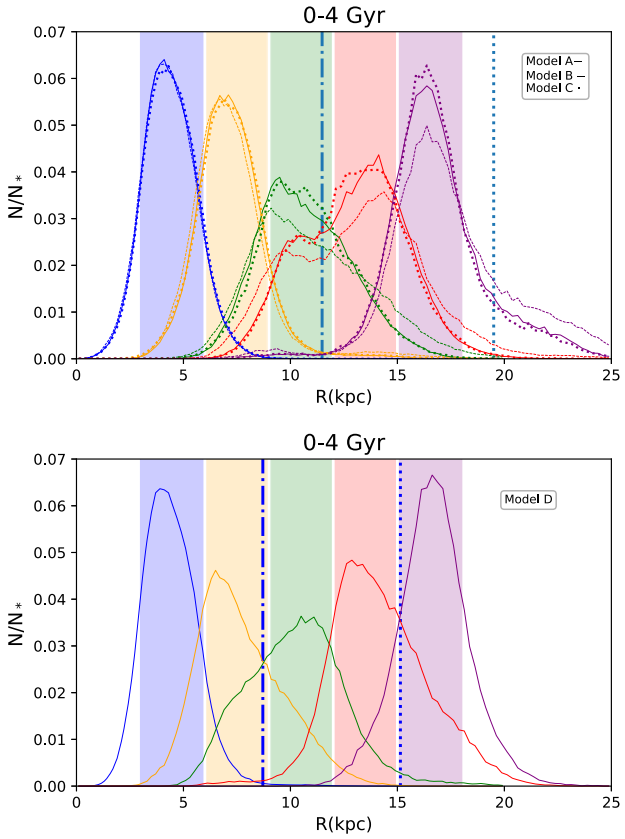

Figure 5. Top row shows the histograms of the number of particles for Models A, B, and C consisting of 5 bins of 3 kpc length starting in 3 kpc. The blue dash–dotted and dotted lines correspond to the CR and the OLR of the galaxy. Each coloured bin represents the initial radii and the curves are the distribution of the same particles after 4 Gyr. The green and red bins are located around the CR resonance, it is clear that the dispersion of particles is larger in this zone than in other places for all models. However, Model B (dashed lines) spreads more particles originally in the green and red coloured bins to other places. Bottom row is the same than top row, but only for Model D, where the resonances are placed in other zones due to the different pattern speed of the spiral arms. Histograms are normalized to the initial (t_0) number of particles.

For Model A, the 50, 55, and 41 per cent of the particles originally found at the third, fourth, and fifth bins (9–12, 12–15, and 15–18 kpc, respectively) at $t = 0$ Gyr, are spread beyond their initial bin. These numbers are slightly different for the Model C, but not enough to make a big difference. Instead, Model B has 59, 62, and 50 per cent of particles that leave their original radial bin, showing a difference in the behaviour of the particles around the main resonances of the system. This model has an increment about 10 per cent of particles that migrate compared to the Model A. For the Model D, the bins around CR are the second, third, and fourth, and the spread particles are 50, 47, and 34 per cent, respectively, as we mention before, this comparison is not straightforward due to the differences in the resonances positions.

4 DISCUSSION AND CONCLUSIONS

The study of radial migration has been addressed and analysed in different scenarios by several authors. For instance, star clusters can migrate to the inner region of our Galaxy, resulting in a fast disruption of these stellar systems due to a strong tidal field (Fujii & Baba 2012). On the contrary, while migrating from the inner parts of the disc up to $\sim$ 5–8 kpc, open clusters are less prone to tidal disruption. Therefore, in the solar neighbourhood, their metallicity is higher than the metallicity of the open clusters that were born there (Anders et al. 2017). Even more, a significant fraction of open clusters in the Milky Way can experience radial migration of about 1.5 kpc Gyr^{-1} (Chen & Zhao 2020).

Also, considering the framework of an infalling galaxy satellite, this will induce the formation of spiral arms and, hence, an increase in the stellar radial migration due to these non-axisymmetric perturbations. This would add considerable dispersion to the age–metallicity relationship in the solar neighbourhood and in the outer parts of the disc, but there is also a considerable radial and vertical heating (Bird, Kazantzidis & Weinberg 2012). In addition, a large number of old metal-poor high-[α/Fe] stars can be found in the solar neighbourhood due to radial mixing, caused by mergers and the subsequent formation of a central bar (Minchev, Chiappini & Martig 2013). Further, a warp and the spiral structure in the external parts caused by a perturbing satellite on to the Galactic disc flatten the metallicity gradients due to stellar migration (Quillen et al. 2009).

It is important to have in mind that radial migration can be studied in different ways; however, this work focuses on the effect of radial migration on individual stars and isolated galaxies, and in a future work we will study the MDF as a clue to radial migration.

We performed a series of simulations using a fully analytical galactic model of a late-type galaxy, to study the effect of the structural and dynamical parameters of the spiral arms on radial migration. We introduce adiabatically the spiral arms potential during the first Gyr to avoid a spurious response of the stellar distribution. To isolate the individual effect of each parameter of the spiral arms model, we carry out simulations where we varied, with respect to our fiducial Model A, the spiral radial scale length (Model B), the pitch angle (Model C), and the pattern speed (Model D). We study the changes in L_z, R, and ecc of the disc particles in each model.

We can summarize our main findings as follows:

(i) The larger changes ΔL_z and ΔR occur around CR; meanwhile, the change in eccentricity, Δecc, around this region is smaller compared to its neighbourhood. This indicates that there is radial migration.

(ii) The most important parameter in the production of radial migration turns out to be the radial scale length, $R_{\rm sp}$, of the spiral arms, generating the largest changes in L_z and R around CR and smaller changes in the eccentricity around that region. The 50, 55, and 41 per cent of the particles found at the third, fourth, and fifth bins (9–12, 12–15, and 15–18 kpc, respectively) in Model A are spread beyond their original bin, while these percentages are larger by 10 per cent for Model B (top panel of Fig. 5).
Furthermore, the radial distribution of particles shows a positive (negative) skewness inside (outside) CR, a clear signature due to the spiral arms.

(iii) In our models, there are particles that move inwards or outwards more than 10 kpc. The CR and OLR contribute to those extreme migrators. This behaviour is compatible with the results from the N-body simulations performed by Halle et al. (2018).

This set of simulations with a cosine model for the spiral arms clearly shows that the radial scale length of the spiral arms plays a relevant role in defining at what extent the radial migration affects the stellar orbits of the disc. Additionally, we want to stress that to have effective and lasting radial migration, the spiral arms should be transient (Sellwood & Binney 2002). Nevertheless, using a steady spiral potential we are able to see a restricted radial migration. We

are aware that a sophisticated study, using more realistic and variable potentials for the spiral arms, is necessary. That study should take into account the interplay of the structural and dynamical parameters of the spiral arms, including the chemical information that could provide an improved approach to the analysis of radial migration in disc galaxies.

ACKNOWLEDGEMENTS

We thank the anonymous referee for the review and suggestions that help us to improve this work. GMB acknowledges CONACYT for the PhD fellowship, and L. Martínez-Medina, E. Athanassoula, O. Valenzuela, and L. Aguilar for the interesting discussions and invaluable suggestions. GMB and HV were supported by the DGAPA-PAPIIT grant IN101918. APV acknowledges the DGAPA-PAPIIT grant IG100319. HV acknowledges the support from the Laboratorio Nacional de Supercómputo del Sureste-Conacyt, the Centro Nacional de Supercómputo-IPICYT-Conacyt, and Miztli of the DGTIC-UNAM. This research was partially supported through computational and human resources provided by the LAMOD UNAM project through the clusters Atocatl and Tochtli. LAMOD is a collaborative effort between the IA, ICN, and IQ institutes at UNAM.

DATA AVAILABILITY

The data used in this article will be shared on request to the corresponding author.

REFERENCES

Anders F. et al., 2017, A&A, 600, A70
Arifyanto M. I., Fuchs B., 2006, A&A, 449, 533
Aumer M., Binney J., Schönrich R., 2016, MNRAS, 459, 3326
Bird J. C., Kazantzidis S., Weinberg D. H., 2012, MNRAS, 420, 913
Chen Y. Q., Zhao G., 2020, MNRAS, 495, 2673
Comparetta J., Quillen A. C., 2012, preprint (arXiv:1207.5753)
Contopoulos G., Grosbol P., 1986, A&A, 155, 11
Daniel K. J., Schaffner D. A., McCluskey F., Fiedler Kawaguchi C., Loebman S., 2019, ApJ, 882, 111
de Laverny P., Recio-Blanco A., Worley C. C., De Pascale M., Hill V., Bijaoui A., 2013, The Messenger, 153, 18
Edvardsson B., Andersen J., Gustafsson B., Lambert D. L., Nissen P. E., Tomkin J., 1993, A&A, 500, 391
Eisenstein D. J. et al., 2011, AJ, 142, 72
Fathi K., Beckman J. E., Piñol-Ferrer N., Hernandez O., Martínez-Valpuesta I., Carignan C., 2009, ApJ, 704, 1657
Feltzing S., Bowers J. B., Agertz O., 2020, MNRAS, 493, 1419
Fujii M. S., Baba J., 2012, MNRAS, 427, L16
Gaia Collaboration, 2018, A&A, 616, A1
Grand R. J. J., Kawata D., Cropper M., 2012, MNRAS, 426, 167
Grieves N. et al., 2018, MNRAS, 481, 3244
Halle A., Di Matteo P., Haywood M., Combes F., 2018, A&A, 616, A86
Hart R. E., Bamford S. P., Keel W. C., Kruk S. J., Masters K. L., Simmons B. D., Smethurst R. J., 2018, MNRAS, 478, 932
Hayden M. R. et al., 2015, ApJ, 808, 132
Hernquist L., 1990, ApJ, 356, 359
Hernquist L., 1993, ApJS, 86, 389
Hunt J. A. S., Bovy J., 2018, MNRAS, 477, 3945
Hunt J. A. S. et al., 2018a, MNRAS, 474, 95
Hunt J. A. S., Hong J., Bovy J., Kawata D., Grand R. J. J., 2018b, MNRAS, 481, 3794
Hunt J. A. S., Bub M. W., Bovy J., Mackereth J. T., Trick W. H., Kawata D., 2019, MNRAS, 490, 1026
Khoperskov S., Di Matteo P., Haywood M., Gómez A., Snaith O. N., 2020, A&A, 638, A144
Klačka J., Nagy R., Jurči M., 2012, MNRAS, 427, 358
Kubryk M., Prantzos N., Athanassoula E., 2013, MNRAS, 436, 1479
Loebman S. R., Debattista V. P., Nidever D. L., Hayden M. R., Holtzman J. A., Clarke A. J., Roškar R., Valluri M., 2016, ApJ, 818, L6
Ma J., Zhao J.-l., Zhang F.-P., Peng Q.-H., 2000, Chin. Astron. Astrophys., 24, 435
Martinez-Medina L. A., Pichardo B., Moreno E., Peimbert A., 2016, MNRAS, 463, 459
Martinez-Medina L. A., Pichardo B., Peimbert A., Carigi L., 2017, MNRAS, 468, 3615
Mata-Chávez M. D., Velázquez H., Pichardo B., Valenzuela O., Roca-Fábrega S., Hernández-Toledo H., Aquino-Ortíz E., 2019, ApJ, 876, 6
Mejía-Narváez A., Sánchez S. F., Lacerda E. A. D., Carigi L., Galbany L., Husemann B., García-Benito R., 2020, MNRAS, 499, 4838
Mikkola D., McMillan P. J., Hobbs D., 2020, MNRAS, 495, 3295
Minchev I., Famaey B., 2010, ApJ, 722, 112
Minchev I., Famaey B., Quillen A. C., Di Matteo P., Combes F., Vlajić M., Erwin P., Bland-Hawthorn J., 2012a, A&A, 548, A126
Minchev I., Famaey B., Quillen A. C., Dehnen W., Martig M., Siebert A., 2012b, A&A, 548, A127
Minchev I., Chiappini C., Martig M., 2013, A&A, 558, A9
Miyamoto M., Nagai R., 1975, PASJ, 27, 533
Monari G., Famaey B., Siebert A., 2016a, MNRAS, 457, 2569
Monari G., Famaey B., Siebert A., Grand R. J. J., Kawata D., Boily C., 2016b, MNRAS, 461, 3835
Patsis P. A., Grosbol P., 1996, A&A, 315, 371
Pérez-Villegas A., Pichardo B., Moreno E., Peimbert A., Velázquez H. M., 2012, ApJ, 745, L14
Pérez-Villegas A., Pichardo B., Moreno E., 2013, ApJ, 772, 91
Pérez-Villegas A., Pichardo B., Moreno E., 2015, ApJ, 809, 170
Pichardo B., Martos M., Moreno E., Espresate J., 2003, ApJ, 582, 230
Pichardo B., Martos M., Moreno E., 2004, ApJ, 609, 144
Plummer H. C., 1911, MNRAS, 71, 460
Prantzos N., de Laverny P., Guiglion G., Recio-Blanco A., Worley C. C., 2017, A&A, 606, A132
Press W. H., Teukolsky S. A., Vetterling W. T., Flannery B. P., 1992, Numerical Recipes in FORTRAN. The Art of Scientific Computing. Cambridge Univ. Press, Cambridge
Quillen A. C., Minchev I., Bland-Hawthorn J., Haywood M., 2009, MNRAS, 397, 1599
Roberts W. W. J., Huntley J. M., van Albada G. D., 1979, ApJ, 233, 67
Roškar R., Debattista V. P., Loebman S. R., Ivezić Z., Quinn T. R., 2011, in Johns-Krull C., Browning M. K., West A. A., eds, ASP Conf. Ser. Vol. 448, 16th Cambridge Workshop on Cool Stars, Stellar Systems, and the Sun. Astron. Soc. Pac., San Francisco, p. 371
Ruiz-Lara T. et al., 2017, A&A, 604, A4
Sánchez-Menguiano L. et al., 2018, A&A, 609, A119
Schönrich R., Binney J., 2009, MNRAS, 396, 203
Sellwood J. A., Binney J. J., 2002, MNRAS, 336, 785
Tsujimoto T., Baba J., 2020, ApJ, 904, 137
Vera-Ciro C., D'Onghia E., Navarro J., Abadi M., 2014, ApJ, 794, 173
Vera-Ciro C., D'Onghia E., Navarro J. F., 2016, ApJ, 833, 42
Wielen R., Fuchs B., Dettbarn C., 1996, A&A, 314, 438
Yu S.-Y., Ho L. C., 2020, ApJ, 900, 150
Zhuang Y., Leaman R., van de Ven G., Zibetti S., Gallazzi A., Zhu L., Falcón-Barroso J., Lyubenova M., 2019, MNRAS, 483, 1862

This paper has been typeset from a TEX/LATEX file prepared by the author.